Inorganic Chemistry

pubs.acs.org/IC

Article

Spatially Ordered Arrangement of Multifunctional Sites at Molecule Level in a Single Catalyst for Tandem Synthesis of Cyclic Carbonates

Shan-Chao Ke,[#] Ting-Ting Luo,[#] Gang-Gang Chang,[*] Ke-Xin Huang, Jia-Xin Li, Xiao-Chen Ma, Jian Wu, Jian Chen, and Xiao-Yu Yang[*]

Cite This: https://dx.doi.org/10.1021/acs.inorgchem.9b02952

Read Online

ACCESS | Metrics & More | Article Recommendations | Supporting Information

ABSTRACT: With fossil energy resources increasingly drying up and gradually causing serious environmental impacts, pursuing a tandem and green synthetic route for a complex and high-value-added compound by using low-cost raw materials has attracted considerable attention. In this regard, the selective and efficient conversion of light olefins with CO_2 into high-value-added organic cyclic carbonates (OCCs) is of great significance owing to their high atom economy and absence of the isolation of intermediates. To fulfill this expectation, a multifunctional catalytic system with controllable spatial arrangement of varied catalytic sites and stable texture, in particular, within a single catalyst, is generally needed. Here, by using a stepwise electrostatic interaction strategy, imidazolium-based ILs and Au nanoparticles (NPs) were stepwise immobilized into a sulfonic group grafted MOF to construct a multifunctional single catalyst with a highly ordered arrangement of catalytic sites. The Au NPs and imidazolium cation are separately responsible for the selective epoxidation and cycloaddition reaction. The mesoporous cage within the MOF enriches the substrate molecules and provides a confined catalytic room for the tandem catalysis. More importantly, the highly ordered arrangement of the varied active sites and strong electrostatic attraction interaction result in the intimate contact and effective mass transfer between the catalytic sites, which allow for the highly efficient (>74% yield) and stable (repeatedly usage for at least 8 times) catalytic transformation. The stepwise electrostatic interaction strategy herein provides an absolutely new approach in fabricating the controllable multifunctional catalysts, especially for tandem catalysis.

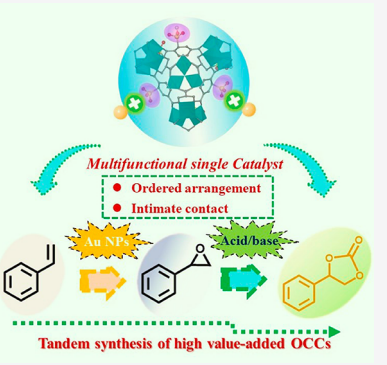

INTRODUCTION

Tandem catalysis that facilitates a series of consecutive catalytic reactions to perform in a concurrent behavior has been regarded as one of the most environmentally friendly processes for the preparation of complex and high-value compounds from low-cost and commercially available raw materials.[1−3] Compared to a traditional stepwise synthesis process, many isolation and purification processes for the following conversion steps are avoided. The tandem catalysis, especially auto-tandem catalysis catalyzed by totally different kinds of catalytic sites, has meanwhile significantly spurred the exploitation of multifunctional catalysts.[4−8]

Organic cyclic carbonates (OCCs) have attracted an increasing market due to their broad application as monomers, aprotic polar solvents, and fine chemical intermediates.[9,10] The selective and efficient conversion of light olefins with CO_2 into high-value-added OCCs has attracted great interest from chemists owing to their high atom economy and absence of the isolation of intermediates, especially considering the low-cost and commercially available light olefins and the increasing worldwide greenhouse effect.[11−16] Generally, the direct oxidative carboxylation of light olefins with CO_2 involves two mechanistically distinct catalytic processes, i.e., the successive epoxidation and cycloaddition process, which requires distinctly different catalytic sites to drive the individual processes. Although extensive homogeneous/heterogeneous catalysts have been introduced to successfully perform the single-step reaction, the tandem catalysis of OCCs catalyzed by multifunctional catalysts has been seldom reported and exhibits poor efficiency due to the thermodynamic and kinetic incompatibility of the individual reactions in the same reaction condition.[17−19] Therefore, the development of a suitable multifunctional catalyst system with excellent selectivity for oxidation of olefins to epoxides and significant affinity to activate inert CO_2 is highly demanded.[20−24]

Ionic liquids (ILs), as a kind of green solvent, are regarded as potential candidates for CO_2 capture due to their low vapor pressure, high stability, and the unique affinity to CO_2.[25−28] However, the complicated recycling process after each reaction due to their liquid nature severely hampers their large-scale application. Metal nanoparticles (MNPs), especially Au NPs, have received a staggering degree of attention due to their high

Received: October 5, 2019

chemical activities and specificities which can play positive roles in olefins selective epoxidation.[29] Generally, the critical bottleneck lies in the dispersion, particle size, and stability (leaching/sintering resistance).[30,31] The simultaneous incorporation of ILs and Au NPs in a porous support, we believe, can be effectively utilized to realize the autotandem synthesis while resolving the deficiency in the individual catalytic sites. In this regard, metal−organic frameworks (MOFs) have been demonstrated to be promising hosts.[32,33] The ultrahigh porosity and well-defined structure could effectively confine the active sites and weaken their leaching and aggregation tendency. Besides, the large pore space can also facilitate mass transfer and diffusion of substrates or products.[34−40] Furthermore, to ensure highly efficient and sustainable synthesis of OCCs, the main challenge for the fabrication of multifunctional catalyst has been beyond the simple selection and incorporation of two or more catalytic sites within MOFs but instead includes a suitable spatial arrangement for distinct catalytic sites. For example, an intimacy distance and ordered distribution according to the reaction sequence between the varied active sites within a single catalyst can ensure the real-time and effective mass transfer between the sequential reactions, which are the major problems in the core−shell structured catalysts or multiple catalysts by physical mixture due to resistance in the shells or the chemical/physical interface.[41−44] In addition, a strong interaction between the catalytic sites and support can effectively stabilize the active sites to make sure the repeated usage from the viewpoint of practical applications.

Bearing all these considerations in mind, herein, imidazolium-based ILs and Au NPs were stepwise immobilized into a sulfonic group grafted MOF, MIL-101(Cr), to construct a multifunctional single catalyst via a stepwise ion exchange and impregnation method. Note that the stepwise electrostatic attraction interaction between the electronegative MOF, electropositive imidazolium cation, and the electronegative Au NPs in the resulted composite single catalyst ensure the stable and highly ordered arrangement of imidazolium cation, Au NPs, and the sulfonic group within the MOF (Scheme 1). In this resulting single-composite catalyst Au@[IM^+]/[MIL-101-SO_3^-], the highly dispersed and ultrafine Au sites can catalyze the selective epoxidation reaction, and the imidazolium cation within the ILs system can provide high affinity for CO_2 and simultaneously function as base sites for the cycloaddition reaction. The mesoporous cage in MIL-101(Cr) can enrich the substrate molecules and provide a confined catalytic room for the tandem catalysis, and the remaining sulfonic group and Cr^{3+} can also act as acid sites to activate the light olefins and CO_2. More importantly, the highly ordered arrangement of the varied active sites and strong electrostatic attraction interaction between each other can ensure the stable and highly efficient catalytic transformation. As a result, the Au@[IM^+]/[MIL-101-SO_3^-] exhibited excellent catalytic activity with complete conversion and >74% yield toward the styrene carbonate in the one-pot oxidative carboxylation of styrene. Remarkably, the catalytic activity was largely retained, and the structure stability was maintained even after successive eight cycles.

Scheme 1. Illustration Showing the Arrangement Style of Au@[IM^+]/[MIL-101-SO_3^-] and Its Application for Tandem Fabrication of Cyclic Carbonates

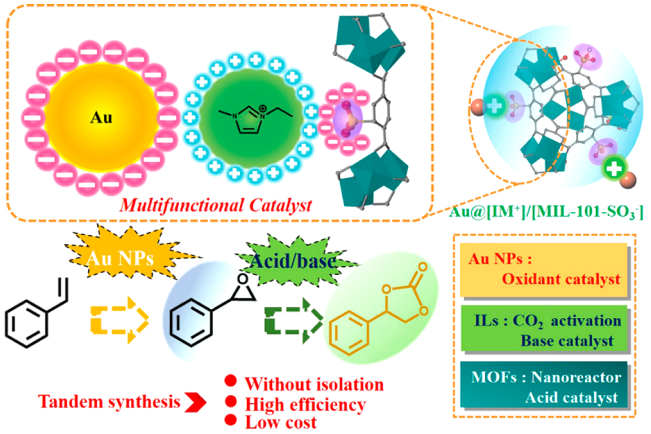

EXPERIMENTAL SECTION

Materials. Monosodium 2-sulfoterephthalic acid ($H_2BDC-SO_3Na$) was acquired from TCI Development Co. Chromium nitrate nonahydrate ($Cr(NO_3)_3·9H_2O$), hydrofluoric acid (HF), hydrochloric acid (HCl), *tert*-butyl hydroperoxide (TBHP), and other commercially available solvents were obtained in high purity from Sinopharm Chemical Reagent Co. 1-Ethyl-3-methyl imidazolium bromide (ILs), styrene, and styrene oxide were obtained from Aladdin Industrial Co. Tetrabutylammonium bromide (TBABr) and chloroauric acid ($HAuCl_4$) were purchased from Beijing InnoChem Science and Technology Co. All commercial chemicals were used without further purification unless otherwise mentioned.

Characterization. Surface area analysis of the various materials was measured by N_2 adsorption/desorption isotherms using a Tristar II 3020 instrument, and the CO_2 adsorption was obtained at 298 K. The crystallinity and phase purity of the samples were obtained by an X-ray diffractometer (XRD) instrument (D8 Advance, Bruker). The surface morphology and frame size of Au@[IM^+]/[MIL-101-SO_3^-] were studied using a field-emission scanning electron microscope (FESEM, S-4800, HITACHI) and a transmission electron microscope (TEM, JEOL-2100F). The loading amount of Au NPs in varied catalysts were determined by inductively coupled plasma−atomic emission spectroscopy (ICP-AES, Prodigy7). IR spectra were recorded on a Bruker VerTex 80v spectrometer. The types of acid sites within various samples were investigated by IR analysis of pyridine adsorption. X-ray photoelectron spectroscopy (XPS) experiments were conducted using a PHI Quantera II instrument (ULVAC-PHI, Japan). Zeta potentials were measured by the electrophoretic mobility of particles in an electric field.

Synthesis of MIL-101-SO_3H. MIL-101-SO_3H was synthesized based on the previous literature with minor modifications.[45] Specifically, a mixture of $Cr(NO_3)_3·9H_2O$ (2.00 g, 5 mmol), $H_2BDC-SO_3Na$ (2.70 g, 10 mmol), and HF (48−51 wt %, 0.3 mL) was dispersed in deionized water (30 mL) and then transferred to a Teflon-capped autoclave. The solution was heated at 190 °C for 24 h and slowly cooled to room temperature. After centrifugation, the as-synthesized solid was washed with deionized water and methanol in sequence to eliminate the unreacted $H_2BDC-SO_3Na$ trapped in the pores of MOF and was dried under vacuum. Then, the obtained solid powder of MIL-101-SO_3Na was postsynthetically acidified in dilute HCl at 80 °C for 12 h. Finally, the resultant green powder was washed and dried at 150 °C for 12 h for further use.

Synthesis of [IM^+]/[MIL-101-SO_3^-]. The incorporation of ILs into MIL-101-SO_3H was realized by using a simple ion exchange method. In a typical synthesis, 100 mg of MIL-101-SO_3H and 94 mg of ILs were dispersed in 10 mL of deionized water; the suspension was stirred at 22 °C for 3 h before imidazolium-modified MIL-101-SO_3H was separated from the solution. Then, the solid was washed with EtOH and desiccated under vacuum. Note that due to the space resistance, it is hard to totally exchange the $-SO_3H$ group. In order to exchange the $-SO_3H$ group as much as possible, the dosage of ILs was excessive during the preparation of [IM^+]/[MIL-101-SO_3^-]. EDX

https://dx.doi.org/10.1021/acs.inorgchem.9b02952
Inorg. Chem. XXXX, XXX, XXX−XXX

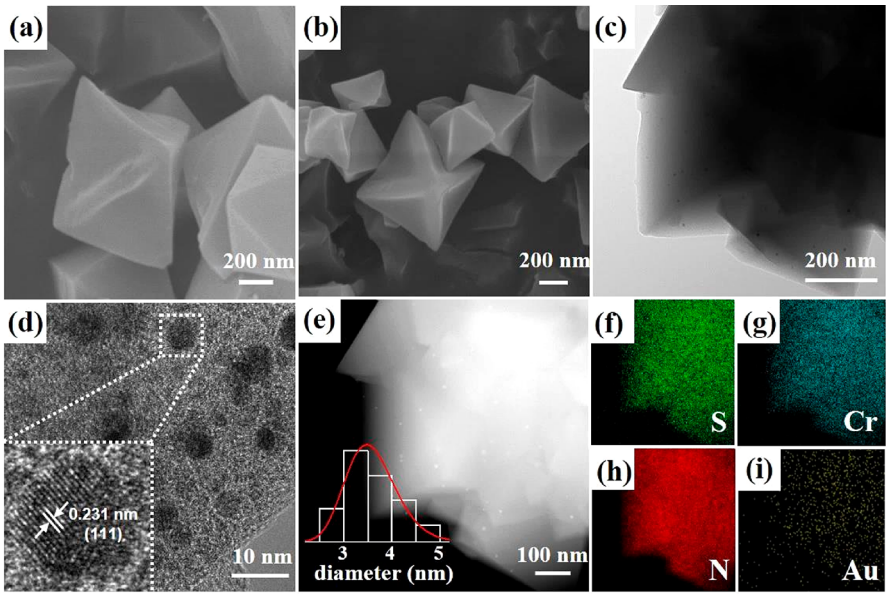

Figure 1. SEM of (a) MIL-101-SO_3H and (b) Au@[IM^+]/[MIL-101-SO_3^-]; (c) TEM images and (d) magnified STEM images of Au@[IM^+]/[MIL-101-SO_3^-]; (e) HAADF-STEM images of Au@[IM^+]/[MIL-101-SO_3^-], where the inset in (e) is the corresponding size distribution of Au NPs; and EDS mapping (f–i) images of Au@[IM^+]/[MIL-101-SO_3^-].

results (Figure S1) showed that the atomic fraction of N and S was 17.13 and 10.75, respectively, which demonstrated that about 80% of the $-SO_3H$ group within MIL-101-SO_3H was exchanged.

Synthesis of *x* wt % Au@[IM^+]/[MIL-101-SO_3^-]. Supported Au catalysts with varied loading amounts were prepared by a double-solvents method. To be specific, the activated [IM^+]/[MIL-101-SO_3^-] was well-dispersed in cyclohexane, and after it sonicated for 10 min until it become homogeneous, different volumes of aqueous $HAuCl_4$ solution were added; the mixture was stirred for 3 h. After filtration, the solid was washed with excess EtOH and dried at 80 °C under vacuum. Finally, the as-prepared Au^{3+} infiltrated [IM^+]/[MIL-101-SO_3^-] was reduced under a 50 mL/min flow of 10% H_2/Ar at 200 °C for 2 h. ICP-AES results revealed that the Au loading amount in the Au@[IM^+]/[MIL-101-SO_3^-] was 0.30, 0.09, and 0.06 wt %, respectively. Various control catalysts were also synthesized for comparison.

Synthesis of Au NPs. The highly dispersed Au NPs were prepared based on a previous report with minor modifications.[46] Specifically, 5 mL of 0.5 mmol/L $HAuCl_4$ was well-dispersed in 5 mL of 0.2 mol/L CTAB solution. After sonication for 10 min, 0.6 mL of 0.01 mol/L $NaBH_4$ was injected, and the mixture was stirred vigorously. The stirring was stopped after the solution color changed from yellow to brownish, and the solution was spun down at 9000 rpm for 15 min and stored in 10 mL of DMF for further use.

Catalytic Tests. In a typical experiment, styrene (50 mg) was well dispersed into 4 mL of solvent containing 1 mL of TBHP followed by addition of the catalysts. After sonication for 5 min, the obtained solution was magnetically stirred at 600 rpm in a stainless-steel autoclave filled with 1 atm O_2 at 80 °C for a period of time to finish the oxidative reaction. Subsequently, 50 mg of TBABr was added to the autoclave; following this, the autoclave was purged with CO_2 eight times and the pressure was set at 10 atm for the following CO_2 cycloaddition process. After the reaction was finished, the reaction solutions were analyzed by gas chromatography (GC, Agilent 7890B) instrumentation equipped with an HP-5 capillary column. The products were identified by GC-MS (Agilent 6890*N*/5975) or ^1H NMR spectra. For recyclable tests, the catalyst was isolated after the reaction was completed. Then, the catalyst was washed with DMF and EtOH several times and heated at 80 °C under vacuum for the next reaction run with reaction conditions consistent with those described above.

RESULTS AND DISCUSSION

As shown in Scheme S1, the imidazolium-based ILs were first immobilized into the MIL-101-SO_3H by ion exchange strategy; then, the ultrafine Au NPs were fixed to the framework by electrostatic interaction with the doped imidazolium cation to construct a stable multifunctional single catalyst Au@[IM^+]/[MIL-101-SO_3^-]. Catalysts with varied Au loadings (0.06, 0.09, and 0.30 wt %) were synthesized for comparison, and 0.30 wt % was chosen as a representative sample for detailed description. The powder XRD patterns of the as-synthesized Au@[IM^+]/[MIL-101-SO_3^-] matched well with the reported patterns of pristine MIL-101-SO_3H (Figure S2A), which indicated the retention of structural integrity after the introduction of ILs and Au NPs. In addition, peaks that referred to Au NPs were too weak to be observed, presumably because of their low concentrations or small size. The surface morphology and structure of the prepared composite catalyst were studied by SEM measurement. As shown in Figure 1b, Au@[IM^+]/[MIL-101-SO_3^-] exhibited regular octahedral-shaped crystals similar to the parent material (Figure 1a). To evaluate the surface areas and pore character, N_2 sorption at 77 K was performed for various samples, and the results were displayed in Figure S2B and Table S1. All adsorption–desorption isotherms showed a type-I shape with a sharp sorption amount at low pressure, indicating that the porous character of Au@[IM^+]/[MIL-101-SO_3^-] was well-inherited from the parent host. Besides, the appreciable decrease of surface area and the slight decrease of mesoporous size (Figure S3) compared to that of the original MIL-101-SO_3H indicated the successful doping of ILs and Au NPs.

The particle size and dispersion of Au NPs within the Au@[IM^+]/[MIL-101-SO_3^-] were characterized by TEM analysis, and the results were shown in Figure 1. As shown in Figure 1e, the ultrasmall Au NPs with an average diameter of ~3.4 nm were well dispersed on the framework, which confirmed that Au NPs were largely trapped inside the framework considering the size of typical mesoporous cage owned by MIL-101-SO_3H (2.9 and 3.4 nm). The high-

https://dx.doi.org/10.1021/acs.inorgchem.9b02952
Inorg. Chem. XXXX, XXX, XXX–XXX

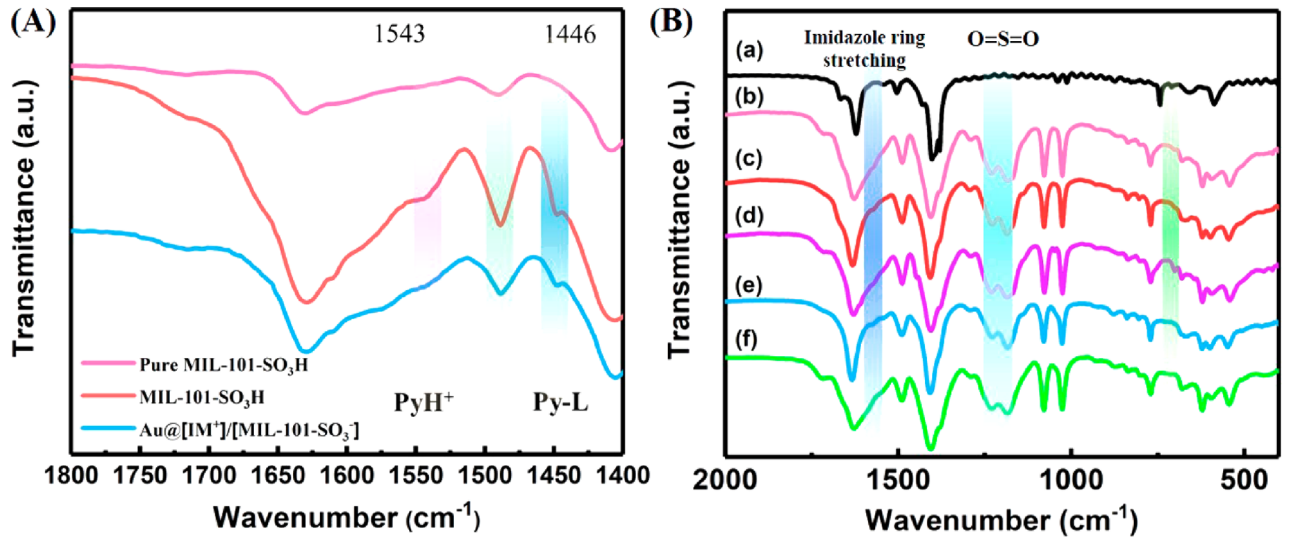

Figure 2. Infrared spectra of pyridine adsorption (A) and the infrared spectra (B) of (a) MIL-101; (b) 0.06 wt %, (c) 0.09 wt %, (d) 0.3 wt % Au@[IM^+]/[MIL-101-SO_3^-]; (e) [IM^+]/[MIL-101-SO_3^-]; and (f) MIL-101-SO_3H.

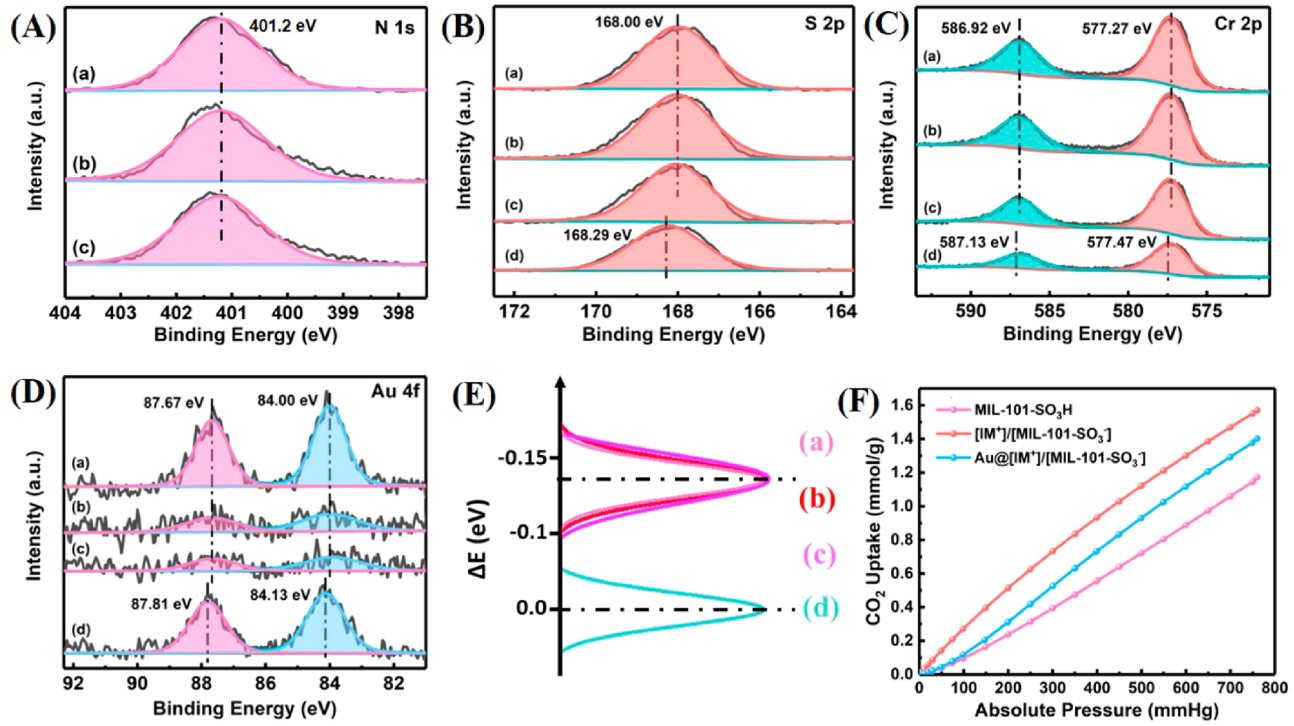

Figure 3. High-resolution N 1s XPS spectra (A), S 2p XPS spectra (B), Cr 2p XPS spectra (C), and Au 4f (D), and relative shift of Au $4f_{5/2}$ (E) for (a) 0.30, (b) 0.09, and (c) 0.06 wt % Au@[IM^+]/[MIL-101-SO_3^-] and (d) Au@MIL-101-SO_3H. The CO_2 uptakes at room temperature (F) of various samples.

resolution TEM image (Figure 1d) demonstrated the polycrystalline structure of the Au NPs with lattice fringes of 0.23 nm, which could be assigned to the (111) planes of the cubic Au NPs. Besides, EDX elemental mapping analysis (Figure 1f–i) showed that N and Au were well distributed within the framework, further indicating the successful introduction of imidazole cation and Au NPs. Note that the absence of Br as revealed by the EDX elemental analysis identified the successful ion exchange of 1-ethyl-3 methyl imidazolium bromide with an $-SO_3H$ group. Moreover, the successful ion exchange of 1-ethyl-3- methyl imidazolium bromide with the $-SO_3H$ group was further confirmed by using FT-IR experiments of pyridine adsorption. As shown in Figure 2A, after adsorption of pyridine, the band at 1543 cm^{-1} related to the stretching vibrations of C—C (N) weakened obviously. Such decrease suggested that the content of accessible Brønsted acid sites within Au@[IM^+]/[MIL-101-SO_3^-] decreased after the introduction of the imidazolium cation, thus resulting in the reduction of PyH^+ composite that formed by pyridine adsorption on Brønsted acid sites. In contrast, the band that appeared at 1446 cm^{-1} corresponding to the Py-L generated by pyridine adsorption on Lewis acid sites showed no obvious changes, which indicated that the

https://dx.doi.org/10.1021/acs.inorgchem.9b02952
Inorg. Chem. XXXX, XXX, XXX−XXX

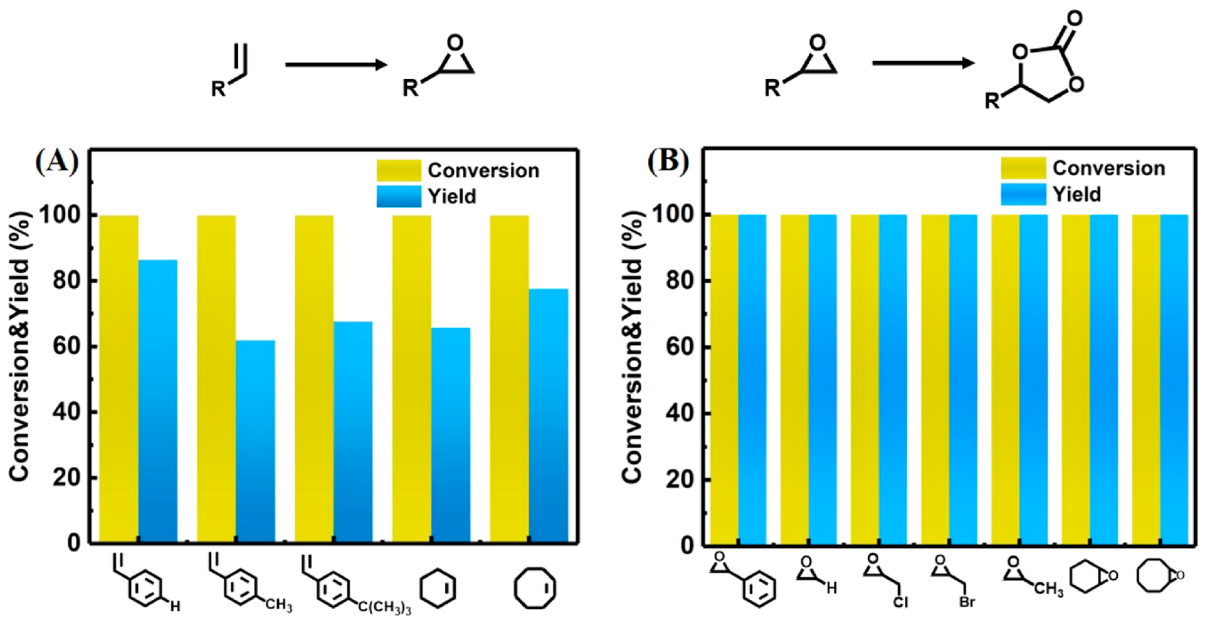

Figure 4. Performance of different substrates in the individual reaction. Reaction conditions: (A) 50 mg of substrate, 50 μL of dodecane, 20 mg of catalyst, 4 mL of DMF, 1 mL of TBHP, 0.1 MPa O_2, 80 °C, stirring at 600 rpm; (B) 50 mg of substrate, 50 μL of dodecane, 20 mg of catalyst, 4 mL of DMF, 1 MPa CO_2, 50 mg of TBABr, 80 °C, stirring at 600 rpm.

Table 1. Oxidative Carboxylation Performance of Different Substrate in the Different Reaction Condition[a]

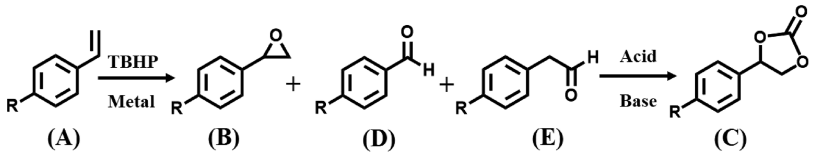

				yield [%]				
entry	catalyst	R	$A_{conv.}$[%]	B	C	D	E	others
1	Au@[IM$^+$]/[MIL-101-SO_3^-]	H	>99	11.9	74.5	5.2	trace	8.3
2	0.09 wt % Au@[IM$^+$]/[MIL-101-SO_3^-]	H	>99	14.8	67.4	10.1	trace	7.9
3	0.06 wt % Au@[IM$^+$]/[MIL-101-SO_3^-]	H	>99	13.6	61.1	15.3	trace	10.1
4	Au@MIL-101-SO_3H	H	>99	17.7	47.8	10.9	trace	23.5
5	Au@ILs/MIL-101	H	>99	25.4	52.8	9.7	trace	12.0
6	Au NPs+ ILs	H	>99	36.2	16.8	36.7	trace	10.3
7	[IM$^+$]/[MIL-101-SO_3^-]	H	trace	trace	trace	trace	trace	trace
8	Au NPs+ ILs+ MIL-101-SO_3H	H	>99	28.3	trace	58.6	trace	13.1
9	Au@[IM$^+$]/[MIL-101-SO_3^-]	CH_3	>99	46.6	9.3	34.5	trace	9.6
10	Au@[IM$^+$]/[MIL-101-SO_3^-]	OCH_3	>99	trace	trace	22.3	trace	79.7
11	Au@[IM$^+$]/[MIL-101-SO_3^-]	$C(CH_3)_3$	>99	trace	trace	67.6	trace	32.4
12	Au@[IM$^+$]/[MIL-101-SO_3^-]	F	>99	42.2	trace	25.0	trace	32.8
13	Au@[IM$^+$]/[MIL-101-SO_3^-][b]	/	>99	77.6	trace	trace	trace	22.4
14	Au@[IM$^+$]/[MIL-101-SO_3^-][c]	/	>99	trace	57.7	trace	trace	42.3

[a]Reaction conditions: (first step) 50 mg of substrate, 50 μL of dodecane, 20 mg of catalyst, 4 mL of DMF, 1 mL of TBHP, 0.1 MPa O_2, 80 °C, stirring at 600 rpm; (second step) 1 MPa CO_2, 50 mg of TBABr, 80 °C, stirring at 600 rpm. [b]Cyclooctene. [c]Cyclohexene.

majority of imidazolium was tethered onto $-SO_3H$ rather than Cr^{3+}.

The Fourier transform infrared spectra (FT-IR) of various samples were collected in Figure 2B. The characteristic bond of O═S═O at 1196 and 1248 cm^{-1} compared with MIL-101 confirmed the existence of $-SO_3H$ groups. Compared to the pristine MIL-101-SO_3H, the peak at 1570 cm^{-1} was ascribed to the stretching vibration of the imidazole ring after the introduction of the imidazolium cation. Besides, a new peak appeared at ~701 cm^{-1} (Figure S4) that could be attributed to the interaction between Au NPs and imidazolium N in the as-prepared Au@[IM$^+$]/[MIL-101-SO_3^-].[47] To further discern the strong interactions between the electronegative MOF, imidazolium cation, and the electronegative Au NPs (Figure S5) in the resulted single catalyst, XPS measurements were performed (Figure S6). First, we employed the high-resolution N 1s spectrum analysis to investigate the states of the N species. The binding energy of the N 1s peak at 401.2 eV in Au@[IM$^+$]/[MIL-101-SO_3^-] (Figure 3A) compared to single type symmetrical pyrrolic N in imidazolium at 400.5 eV illustrated a slight shift to a higher binding energy.[48] The positive displacement confirmed the existence of an interaction

https://dx.doi.org/10.1021/acs.inorgchem.9b02952
Inorg. Chem. XXXX, XXX, XXX−XXX

between the imidazolium cation and the MOF framework. A slight shift to lower binding energies could be observed in S 2p (Figure 3B) and Cr 2p (Figure 3C) spectra, which also confirmed the interaction between $-SO_3^-$ anion and imidazolium cation as well as the interaction between Cr^{3+} and imidazolium, respectively.[49] Meanwhile, the high-resolution Au 4f spectra (Figure 3D) depicted the presence of Au element in the Au@[IM$^+$]/[MIL-101-SO_3^-]. The XPS spectrum showed two peaks at a binding energy of 84.00 and 87.67 eV which could be attributed to the formation of Au^0 $4f_{7/2}$ and $4f_{5/2}$, respectively. Note that the peak intensity of Au was very weak due to the low loading within the composite catalyst, which is consistent with ICP-AES analysis. Compared to the samples without doped ILs, about a ca. 0.13 eV (Figure 3E) slight shift to lower binding energies could be attributed to the strong electron-donating effect of nitrogen atoms to the Au NPs, resulting in more electron-rich Au species.[50,51]

To systematically evaluate the catalytic performance of the single catalyst in the challenging autotandem synthesis of OCCs, we separately tested the individual oxidation of olefins and CO_2 cycloaddition prior to performing the tandem catalysis. The individual catalytic results are shown in Figure 4. We could find that Au@[IM$^+$]/[MIL-101-SO_3^-] exhibited excellent catalytic performance toward the oxidation of styrene with complete conversion and >85% yield. While for the substituted styrene, the reaction process was more complicated; it showed relatively lower selectivity but was still completely reacted. Meanwhile, Au@[IM$^+$]/[MIL-101-SO_3^-] was further evaluated for the individual CO_2 cycloaddition. Prior to performing the reactions, we measured the adsorption capacity of [IM$^+$]/[MIL-101-SO_3^-] toward CO_2. Delightedly, [IM$^+$]/[MIL-101-SO_3^-] showed a much enhanced absorption capacity of CO_2 compared to the initial MIL-101-SO_3H despite having much decreased surface areas (Figure 3F), which could be attributed to the strong affinity of the imidazolium-based ILs to CO_2. The catalytic performance of CO_2 cycloaddition was displayed in Figure 4B, which exhibited excellent catalytic performance toward all the substrate molecules at moderate reaction condition. Subsequently, the tandem catalytic synthesis of styrene carbonate was investigated by using the styrene and CO_2 as the starting material, and the results were shown in Table 1. First, the Au@[IM$^+$]/[MIL-101-SO_3^-] catalysts with varied Au content were evaluated. As shown in Table 1 (entry 1), 0.30 wt % Au@[IM$^+$]/[MIL-101-SO_3^-] possessed the best catalytic activity with higher than 99% conversion of styrene and achieves 74.5% yield toward styrene carbonate. Note that most previously reported catalysts exhibited less than 50% yield to the target product in the oxidative carboxylation of olefins.[52,53] Besides, the main byproducts produced during the aerobic oxidation of olefins were the benzaldehyde due to the oxidation of C=C bond cleavage in accordance with previously published work,[54] whereas the phenylacetaldehyde generated by the rearrangement of styrene oxide was not detected in the current reaction system. Second, various green and common oxidizing agents, e.g., H_2O_2, O_2, and air atmosphere were evaluated to screen out the best oxidizing agents (Figure S7). The pure O_2 showed much higher selectivity to the styrene carbonate than air atmosphere (only 16.8% yield), and the utilization of TBHP as the initiator is a must in order to afford a higher yield of epoxides due to the activation of molecular O_2 by TBHP for olefin epoxidation, which could further promote the next cycloaddition of carbon dioxide to epoxides. When using only O_2 or H_2O_2 as the oxidizing agents, the selectivity to styrene carbonate was negligible and most of the raw material transformed to benzaldehyde. Comparatively, for the blank experiment, the tandem reaction could not happen at all without the addition of catalysts and oxidizing agent. The above results demonstrated that Au@[IM$^+$]/[MIL-101-SO_3^-] was excellent catalyst in catalyzing the tandem synthesis of styrene carbonate, during which pure O_2 and TBHP as the initiator were necessary to guaranty the high yield.

As previously reported,[12] the solvent type, especially the polarity, might have a significant effect on the product distribution. In this regard, we further investigate the effect of solvent in the catalytic oxidative carboxylation of olefins, and various solvents with different polarities were tested. As shown in Figure S8, an excellent conversion of olefin was realized in all the solvents, indicating the high catalytic activity of Au@[IM$^+$]/[MIL-101-SO_3^-] in the oxidation of olefin. The highest yield of styrene carbonate was obtained in the case of DMF (74.5% yield), that with the strongest polarity, whereas the yield toward styrene carbonate decreased sharply with the decrease of solvent polarity; no styrene carbonate was observed when using the nonpolar cyclohexane as the solvent, resulting in benzaldehyde as the undesirable byproduct. Because of the very hydrophilic nature of MIL-101-SO_3H, the reaction that performed in polar solvents exhibited better performance than that in nonpolar solvents. This solvent-driven selectivity control has also been reported in the recent studies.[55,56] Additionally, to identify the crucial role of ILs and Au NPs that has been played by Au@[IM$^+$]/[MIL-101-SO_3^-] in enhancing the one-pot tandem reactions, two contrast catalysts in the absence of ILs or Au NPs were separately synthesized and utilized in the one-pot catalytic reaction. For comparison, when using Au@MIL-101-SO_3H (Table 1 entry 4) and Au@ILs/MIL-101 (Table 1 entry 5) as the catalyst, the yield of styrene carbonate decreased drastically, which demonstrated that the imidazole cation and $-SO_3$H group played an important role in activating the CO_2 molecules. The MOF framework was also essential to obtain a high yield of cyclic carbonate by providing a confined reaction room and in stabilizing the whole catalytic sites (Table 1 entry 6). Similarly, when this reaction was catalyzed by [IM$^+$]/[MIL-101-SO_3^-] (Table 1 entry 7), the tandem reaction could not work at all, indicating the necessity of Au NPs in olefin oxidation. Furthermore, when only a physical mixture of Au NPs, ILs, and MIL-101-SO_3H (Table 1 entry 8) was employed to catalyze this reaction, the selectivity to styrene carbonate was negligible in spite of the complete conversion, demonstrating the synergetic effects of the integrated composites than the physical mixture. The catalytic applicability of Au@[IM$^+$]/[MIL-101-SO_3^-] toward styrene bearing different functional groups and two cycloolefins were also investigated with the optimized conditions in DMF. As shown in Table 1, all olefins bearing different functional groups were converted completely, which further demonstrated the excellent catalytic performance of Au NPs in olefin oxidation. However, except for 4-methoxystyrene (10% yield) (Table 1 entry 9) and cyclohexene (60% yield) (Table 1 entry 14), other substrates (Table 1 entries 10−13) exhibited negligible yield of corresponding carbonates, resulting in the substituted benzaldehyde as the major byproduct.

Finally, the recyclability of the Au@[IM$^+$]/[MIL-101-SO_3^-] catalyst in one-pot oxidative carboxylation of olefins was also

https://dx.doi.org/10.1021/acs.inorgchem.9b02952
Inorg. Chem. XXXX, XXX, XXX−XXX

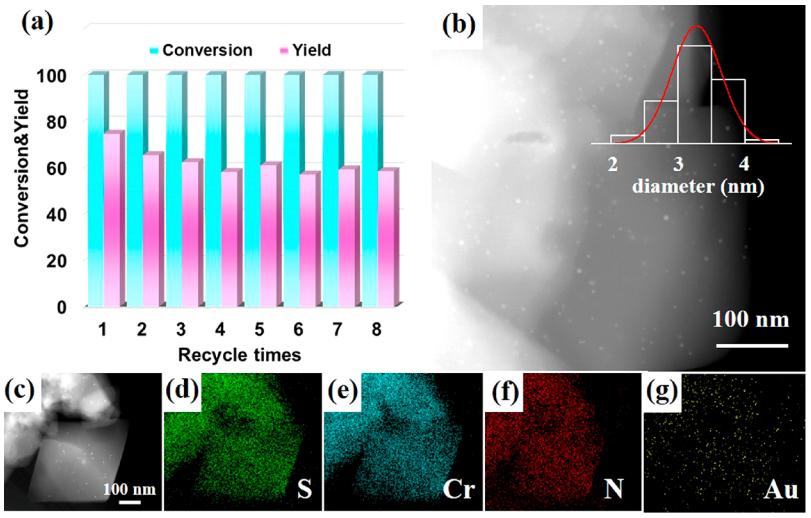

Figure 5. (a) Recycling test of Au@[IM$^+$]/[MIL-101-SO$_3^-$] catalyst. (b) Magnified STEM images; the inset in (b) is the corresponding size distribution of the Au NPs pattern. (c) HAADF-STEM images and EDS mapping (d–g) images of Au@[IM$^+$]/[MIL-101-SO$_3^-$] after eight runs.

Scheme 2. Possible Reaction Mechanism of Oxidative Carboxylation of Styrene

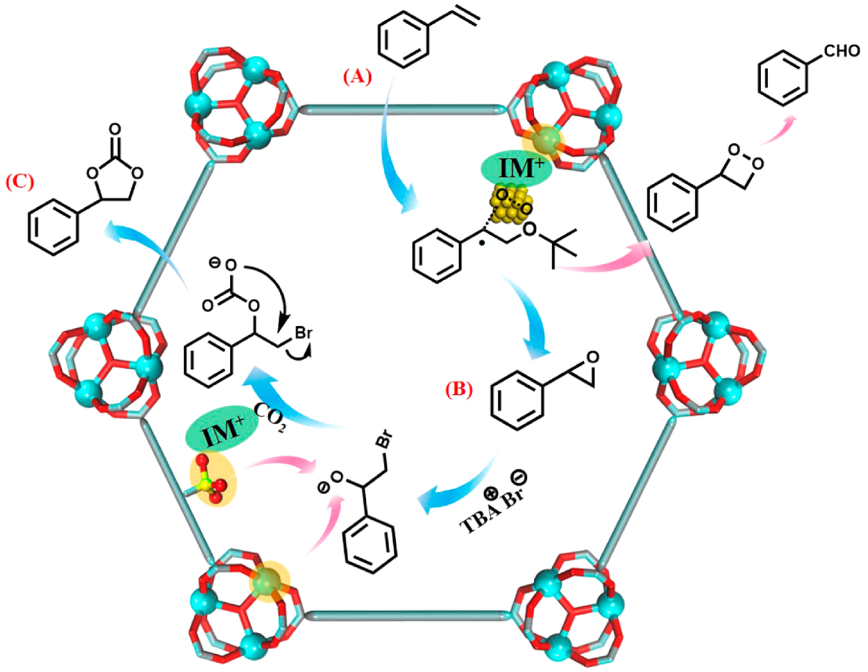

examined. The Au@[IM$^+$]/[MIL-101-SO$_3^-$] was separated from the reaction mixture after each reaction run and reused in the next reaction after it was washed and dried. Remarkably, the catalytic activity of Au@[IM$^+$]/[MIL-101-SO$_3^-$] was well retained for at least eight cycles without an obvious drop in product yield (Figure 5). No significant loss of crystallinity or structural integrity for Au@[IM$^+$]/[MIL-101-SO$_3^-$] was observed from the XRD patterns of the used catalysts (Figure S2A). Besides, the TEM images revealed that the particle size and dispersion degree of Au NPs almost remained unchanged in the recycling test (Figure 4B), which suggested that the excellent chemical and structure stability of the as-prepared multifunctional catalyst benefited from strong electrostatic interaction between the imidazole cation, anionic framework, and Au NPs. Based on the above catalytic results, a tentative mechanism for this one-pot oxidative carboxylation reaction was proposed, which was illustrated in Scheme 2. To be brief, first, the styrene and O_2 were adsorbed on the surface of supported Au NPs, accompanied with the decomposition of TBHP at the surface of Au NPs to form the *tert*-butoxperoxy species, which added electrophilicity to the C=C bond to generate a carbon-centered radical. Then, the carbon-centered radical further underwent migration of oxygen to form the epoxide.[54,57] Meanwhile, the peroxyl radical from the possible involvement of dioxygen could attack the neighboring carbon, removing *tert*-butoxperoxy species and forming the corresponding dioxetane intermediate, which finally contributed to the formation of benzaldehyde through cycloreversion reaction. Second, as for the cycloaddition of epoxide with CO_2, the epoxide first bound with the Brønsted or Lewis acid sites in the MIL-101-SO$_3$H through the O atom of epoxide to activate of the epoxy ring.[58,59] Subsequently, the less-hindered

https://dx.doi.org/10.1021/acs.inorgchem.9b02952
Inorg. Chem. XXXX, XXX, XXX−XXX

carbon of the activated epoxide was then attacked by the Br^- generated from TBABr to open the epoxy ring, which further interacted with CO_2 molecule to form an alkylcarbonate anion. Finally, the corresponding cyclic carbonate was produced through a ring closing step of alkylcarbonate anion.

CONCLUSION

In summary, a stable multifunctional single composite catalyst Au@[IM^+]/[MIL-101-SO_3^-] with a highly ordered and intimate arrangement of active sites was successfully fabricated by using a stepwise electrostatic interaction strategy. The highly ordered arrangement of the imidazolium cation, Au NPs, and the sulfonic group within the MOF and the strong electrostatic attraction interaction between each component form a stable structure and facilitate the close connection between different catalytic sites and effective and efficient mass transfer between the intermediate molecules to speed the reaction process. As a result, the resultant single catalyst exhibited excellent catalytic activity with complete conversion and >74% yield toward the challenging tandem synthesis of the high-value-added product styrene carbonate using low-cost styrene and CO_2 as the starting materials. The catalytic product was solvent dependent, in that the polar solvent contributed to the formation of target product with DMF as the best solvent, while nonpolar solvent mainly resulted in the yield of benzaldehyde as a byproduct. More importantly, the catalytic activity was largely retained (~85% of the initial run) and the structure stability was maintained after eight successive cycles, which benefited from the stepwise electrostatic attraction interaction between the MOF, imidazolium cation, and Au NPs. This novel stepwise electrostatic interaction strategy in fabricating highly ordered multifunctional single catalysts will certainly stimulate more research work on the design of multifunctional catalysts, especially for sustainable chemical synthesis.

ASSOCIATED CONTENT

Supporting Information

The Supporting Information is available free of charge at https://pubs.acs.org/doi/10.1021/acs.inorgchem.9b02952.

XPS results, FTIR spectra, EDS results, zeta potential distributions, N_2 adsorption/desorption results, details of preparation, and catalytic effects of solvent and oxidizing agents (PDF)

AUTHOR INFORMATION

Corresponding Authors

Gang-Gang Chang − *Wuhan University of Technology, Wuhan, China*; orcid.org/0000-0002-8085-6575; Email: changgang2016@whut.edu.cn

Xiao-Yu Yang − *Wuhan University of Technology, Wuhan, China*; Email: xyyang@whut.edu.cn

Other Authors

Shan-Chao Ke − *Wuhan University of Technology, Wuhan, China*

Ting-Ting Luo − *Wuhan University of Technology, Wuhan, China, and Material Research and Testing Center of Wuhan University of Technology, Nanostructure Research Centre, Wuhan, China*

Ke-Xin Huang − *Wuhan University of Technology, Wuhan, China*

Jia-Xin Li − *Wuhan University of Technology, Wuhan, China*

Xiao-Chen Ma − *Wuhan University of Technology, Wuhan, China*

Jian Wu − *Wuhan University of Technology, Wuhan, China*

Jian Chen − *Wuhan University of Technology, Wuhan, China*

Complete contact information is available at: https://pubs.acs.org/10.1021/acs.inorgchem.9b02952

Author Contributions

#These authors contributed equally.

Notes

The authors declare no competing financial interest.

ACKNOWLEDGMENTS

This work was supported by the National Natural Science Foundation of China (21706199, U1662134, 51861135313). We are also grateful to the NRC (Nanostructure Research Centre), Wuhan University of Technology, Wuhan 430070, P.R. China, for its support.

REFERENCES

(1) Huang, Y.-B.; Liang, J.; Wang, X.-S.; Cao, R. Multifunctional metal−organic framework catalysts: synergistic catalysis and tandem reactions. *Chem. Soc. Rev.* **2017**, *46*, 126−157.

(2) Jagadeesan, D. Multifunctional nanocatalysts for tandem reactions: A leap toward sustainability. *Appl. Catal., A* **2016**, *511*, 59−77.

(3) Shindoh, N.; Takemoto, Y.; Takasu, K. Auto-Tandem Catalysis: A Single Catalyst Activating Mechanistically Distinct Reactions in a Single Reactor. *Chem. - Eur. J.* **2009**, *15*, 12168−12179.

(4) Fogg, D. E.; dos Santos, E. N. Tandem catalysis: a taxonomy and illustrative review. *Coord. Chem. Rev.* **2004**, *248*, 2365−2379.

(5) Lohr, T. L.; Marks, T. J. Orthogonal tandem catalysis. *Nat. Chem.* **2015**, *7*, 477.

(6) Venning, A. R.; Kwiatkowski, M. R.; Roque Peña, J. E.; Lainhart, B. C.; Guruparan, A. A.; Alexanian, E. J. Palladium-catalyzed carbocyclizations of unactivated alkyl bromides with alkenes involving auto-tandem catalysis. *J. Am. Chem. Soc.* **2017**, *139*, 11595−11600.

(7) Robert, C.; Thomas, C. M. Tandem catalysis: a new approach to polymers. *Chem. Soc. Rev.* **2013**, *42*, 9392−9402.

(8) Zhao, J.; Hughes, C. O.; Toste, F. D. Synthesis of aromatic ketones by a transition metal-catalyzed tandem sequence. *J. Am. Chem. Soc.* **2006**, *128*, 7436−7437.

(9) Ding, M.; Chen, S.; Liu, X. Q.; Sun, L. B.; Lu, J.; Jiang, H. L. Metal−Organic Framework-Templated Catalyst: Synergy in Multiple Sites for Catalytic CO_2 Fixation. *ChemSusChem* **2017**, *10*, 1898−1903.

(10) Gao, W. Y.; Chen, Y.; Niu, Y.; Williams, K.; Cash, L.; Perez, P. J.; Wojtas, L.; Cai, J.; Chen, Y. S.; Ma, S. Crystal engineering of an nbo topology metal−organic framework for chemical fixation of CO_2 under ambient conditions. *Angew. Chem., Int. Ed.* **2014**, *53*, 2615−2619.

(11) Eghbali, N.; Li, C.-J. Conversion of carbon dioxide and olefins into cyclic carbonates in water. *Green Chem.* **2007**, *9*, 213−215.

(12) Yang, X.; Wu, J.; Mao, X.; Jamison, T. F.; Hatton, T. A. Microwave assisted synthesis of cyclic carbonates from olefins with sodium bicarbonates as the C1 source. *Chem. Commun.* **2014**, *50*, 3245−3248.

(13) Maksimchuk, N. V.; Ivanchikova, I. D.; Ayupov, A. B.; Kholdeeva, O. A. One-step solvent-free synthesis of cyclic carbonates

by oxidative carboxylation of styrenes over a recyclable Ti-containing catalyst. *Appl. Catal., B* **2016**, *181*, 363−370.
(14) Dhakshinamoorthy, A.; Garcia, H. Cascade reactions catalyzed by metal organic frameworks. *ChemSusChem* **2014**, *7*, 2392−2410.
(15) Zhang, S.; Xia, Z.; Zou, Y.; Cao, F.; Liu, Y.; Ma, Y.; Qu, Y. (2019). Interfacial Frustrated Lewis Pairs of CeO_2 Activate CO_2 for Selective Tandem Transformation of Olefins and CO_2 into Cyclic Carbonates. *J. Am. Chem. Soc.* **2019**, *141*, 11353−11357.
(16) Murzin, D. Y. On Spatial Control in Heterogeneous Multifunctional Catalysts. *Catal. Lett.* **2017**, *147*, 613−621.
(17) Mousavi, B.; Chaemchuen, S.; Moosavi, B.; Luo, Z.; Gholampour, N.; Verpoort, F. Zeolitic imidazole framework-67 as an efficient heterogeneous catalyst for the conversion of CO_2 to cyclic carbonates. *New J. Chem.* **2016**, *40*, 5170−5176.
(18) Jiang, Z. R.; Wang, H.; Hu, Y.; Lu, J.; Jiang, H. L. Polar group and defect engineering in a metal−organic framework: synergistic promotion of carbon dioxide sorption and conversion. *ChemSusChem* **2015**, *8*, 878−885.
(19) Wang, X.; Gao, W.-Y.; Niu, Z.; Wojtas, L.; Perman, J. A.; Chen, Y.-S.; Li, Z.; Aguila, B.; Ma, S. A metal−metalloporphyrin framework based on an octatopic porphyrin ligand for chemical fixation of CO_2 with aziridines. *Chem. Commun.* **2018**, *54*, 1170−1173.
(20) Jiang, Y.; Tan, P.; Qi, S. C.; Liu, X. Q.; Yan, J. H.; Fan, F.; Sun, L. B. Metal−Organic Frameworks with Target-Specific Active Sites Switched by Photoresponsive Motifs: Efficient Adsorbents for Tailorable CO_2 Capture. *Angew. Chem., Int. Ed.* **2019**, *58*, 6600−6604.
(21) Sun, L.-B.; Li, A.-G.; Liu, X.-D.; Liu, X.-Q.; Feng, D.; Lu, W.; Yuan, D.; Zhou, H.-C. Facile fabrication of cost-effective porous polymer networks for highly selective CO 2 capture. *J. Mater. Chem. A* **2015**, *3*, 3252−3256.
(22) Ding, M.; Flaig, R. W.; Jiang, H.-L.; Yaghi, O. M. Carbon capture and conversion using metal−organic frameworks and MOF-based materials. *Chem. Soc. Rev.* **2019**, *48*, 2783−2828.
(23) Yang, Q.; Yang, C. C.; Lin, C. H.; Jiang, H. L. Metal−Organic-Framework-Derived Hollow N-Doped Porous Carbon with Ultrahigh Concentrations of Single Zn Atoms for Efficient Carbon Dioxide Conversion. *Angew. Chem., Int. Ed.* **2019**, *58*, 3511−3515.
(24) Ding, M.; Jiang, H.-L. Incorporation of imidazolium-based poly (ionic liquid) s into a metal−organic framework for CO_2 capture and conversion. *ACS Catal.* **2018**, *8*, 3194−3201.
(25) Zhang, X.; Zhang, X.; Dong, H.; Zhao, Z.; Zhang, S.; Huang, Y. Carbon capture with ionic liquids: overview and progress. *Energy Environ. Sci.* **2012**, *5*, 6668−6681.
(26) Yang, Q.; Zhang, Z.; Sun, X.-G.; Hu, Y.-S.; Xing, H.; Dai, S. Ionic liquids and derived materials for lithium and sodium batteries. *Chem. Soc. Rev.* **2018**, *47*, 2020−2064.
(27) Chong, S.; Wang, T.; Cheng, L.; Lv, H.; Ji, M. Metal−Organic Framework MIL-101-NH2-Supported Acetate-Based Butylimidazolium Ionic Liquid as a Highly Efficient Heterogeneous Catalyst for the Synthesis of 3-Aryl-2-oxazolidinones. *Langmuir* **2019**, *35*, 495−503.
(28) Ye, C.; Qi, Z.; Cai, D.; Qiu, T. Design and Synthesis of Ionic Liquid Supported Hierarchically Porous Zr Metal−Organic Framework as a Novel Brønsted−Lewis Acidic Catalyst in Biodiesel Synthesis. *Ind. Eng. Chem. Res.* **2019**, *58*, 1123−1132.
(29) Zou, B.; Hu, C. Synthesis of Cyclic Carbonates from Alkenyl and Alkynyl Substrates. *Chin. J. Chem.* **2017**, *35*, 541−550.
(30) Yang, Q.; Liu, W.; Wang, B.; Zhang, W.; Zeng, X.; Zhang, C.; Qin, Y.; Sun, X.; Wu, T.; Liu, J.; Huo, F.; Lu, J. Regulating the spatial distribution of metal nanoparticles within metal-organic frameworks to enhance catalytic efficiency. *Nat. Commun.* **2017**, *8*, 14429.
(31) Zhu, Q.-L.; Xu, Q. Immobilization of ultrafine metal nanoparticles to high-surface-area materials and their catalytic applications. *Chem.* **2016**, *1*, 220−245.
(32) Fujie, K.; Kitagawa, H. Ionic liquid transported into metal−organic frameworks. *Coord. Chem. Rev.* **2016**, *307*, 382−390.
(33) Luo, Q.-x.; An, B.-w.; Ji, M.; Zhang, J. Hybridization of metal−organic frameworks and task-specific ionic liquids: fundamentals and challenges. *Mater. Chem. Front.* **2018**, *2*, 219−234.
(34) Bao, Z.; Chang, G.; Xing, H.; Krishna, R.; Ren, Q.; Chen, B. Potential of microporous metal−organic frameworks for separation of hydrocarbon mixtures. *Energy Environ. Sci.* **2016**, *9*, 3612−3641.
(35) Chang, G.; Li, B.; Wang, H.; Bao, Z.; Yildirim, T.; Yao, Z.; Xiang, S.; Zhou, W.; Chen, B. A microporous metal−organic framework with polarized trifluoromethyl groups for high methane storage. *Chem. Commun.* **2015**, *51*, 14789−14792.
(36) Chang, G.; Huang, M.; Su, Y.; Xing, H.; Su, B.; Zhang, Z.; Yang, Q.; Yang, Y.; Ren, Q.; Bao, Z.; Chen, B. Immobilization of Ag (i) into a metal−organic framework with−SO $_3$H sites for highly selective olefin−paraffin separation at room temperature. *Chem. Commun.* **2015**, *51*, 2859−2862.
(37) Li, X.; Guo, Z.; Xiao, C.; Goh, T. W.; Tesfagaber, D.; Huang, W. Tandem catalysis by palladium nanoclusters encapsulated in metal−organic frameworks. *ACS Catal.* **2014**, *4*, 3490−3497.
(38) Chen, G.; Wu, S.; Liu, H.; Jiang, H.; Li, Y. Palladium supported on an acidic metal−organic framework as an efficient catalyst in selective aerobic oxidation of alcohols. *Green Chem.* **2013**, *15*, 230−235.
(39) She, H.; Ma, X.; Chang, G. Highly efficient and selective removal of N-heterocyclic aromatic contaminants from liquid fuels in a Ag(I) functionalized metal-organic framework: Contribution of multiple interaction sites. *J. Colloid Interface Sci.* **2018**, *518*, 149−155.
(40) Zhang, X.-L.; Zhang, D.-X.; Chang, G.-G.; Ma, X.-C.; Wu, J.; Wang, Y.; Yu, H.-Z.; Tian, G.; Chen, J.; Yang, X.-Y. Bimetallic (Zn/Co) MOFs-Derived Highly Dispersed Metallic Co/HPC for Completely Hydrolytic Dehydrogenation of Ammonia−Borane. *Ind. Eng. Chem. Res.* **2019**, *58*, 7209−7216.
(41) Cho, H. J.; Kim, D.; Li, J.; Su, D.; Xu, B. Zeolite-encapsulated Pt nanoparticles for tandem catalysis. *J. Am. Chem. Soc.* **2018**, *140*, 13514−13520.
(42) Han, Q.; Qi, B.; Ren, W.; He, C.; Niu, J.; Duan, C. Polyoxometalate-based homochiral metal-organic frameworks for tandem asymmetric transformation of cyclic carbonates from olefins. *Nat. Commun.* **2015**, *6*, 10007.
(43) Liu, X. Y.; Zhang, F.; Goh, T. W.; Li, Y.; Shao, Y. C.; Luo, L.; Huang, W.; Long, Y. T.; Chou, L. Y.; Tsung, C. K. Using a Multi-Shelled Hollow Metal−Organic Framework as a Host to Switch the Guest-to-Host and Guest-to-Guest Interactions. *Angew. Chem.* **2018**, *130*, 2132−2136.
(44) Bai, D.; Jing, H. Aerobic oxidative carboxylation of olefins with metalloporphyrin catalysts. *Green Chem.* **2010**, *12*, 39−41.
(45) Li, H.; Wang, K.; Feng, D.; Chen, Y. P.; Verdegaal, W.; Zhou, H. C. Incorporation of Alkylamine into Metal−Organic Frameworks through a Brønsted Acid−Base Reaction for CO_2 Capture. *ChemSusChem* **2016**, *9*, 2832−2840.
(46) Pan, J.; Zhang, L.; Zhang, S.; Shi, Z.; Wang, X.; Song, S.; Zhang, H. Half-Encapsulated Au Nanorods@ CeO_2 Core@ Shell Nanostructures for Near-Infrared Plasmon-Enhanced Catalysis. *ACS Appl. Nano. Mater.* **2019**, *2*, 1516−1524.
(47) Nellaiappan, S.; Kumar, A. S.; Nisha, S.; Chandrasekara Pillai, K. In-situ preparation of Au (111) oriented nanoparticles trapped carbon nanofiber-chitosan modified electrode for enhanced bifunctional electrocatalysis and sensing of formaldehyde and hydrogen peroxide in neutral pH solution. *Electrochim. Acta* **2017**, *249*, 227−240.
(48) Lee, W. J.; Lim, J.; Kim, S. O. Nitrogen dopants in carbon nanomaterials: defects or a new opportunity? *Small* **2017**, *1*, 1600014.
(49) Sun, Y.; Huang, H.; Vardhan, H.; Aguila, B.; Zhong, C.; Perman, J. A.; Al-Enizi, A. M.; Nafady, A.; Ma, S. Facile Approach to Graft Ionic Liquid into MOF for Improving the Efficiency of CO_2 Chemical Fixation. *ACS Appl. Mater. Interfaces* **2018**, *10*, 27124−27130.
(50) Singuru, R.; Dhanalaxmi, K.; Shit, S. C.; Reddy, B. M.; Mondal, J. Palladium Nanoparticles Encaged in a Nitrogen-Rich Porous Organic Polymer: Constructing a Promising Robust Nanoarchitecture for Catalytic Biofuel Upgrading. *ChemCatChem* **2017**, *9*, 2550−2564.

https://dx.doi.org/10.1021/acs.inorgchem.9b02952
Inorg. Chem. XXXX, XXX, XXX−XXX

(51) Tsumori, N.; Chen, L.; Wang, Q.; Zhu, Q.-L.; Kitta, M.; Xu, Q. Quasi-MOF: exposing inorganic nodes to guest metal nanoparticles for drastically enhanced catalytic activity. *Chem.* **2018**, *4*, 845−856.
(52) Sun, J.; Fujita, S.-i.; Bhanage, B. M.; Arai, M. One-pot synthesis of styrene carbonate from styrene in tetrabutylammonium bromide. *Catal. Today* **2004**, *93*, 383−388.
(53) Sun, J.; Fujita, S.-i.; Bhanage, B. M.; Arai, M. Direct oxidative carboxylation of styrene to styrene carbonate in the presence of ionic liquids. *Catal. Commun.* **2004**, *5*, 83−87.
(54) Dhakshinamoorthy, A.; Alvaro, M.; Garcia, H. Aerobic oxidation of styrenes catalyzed by an iron metal organic framework. *ACS Catal.* **2011**, *1*, 836−840.
(55) Chen, X.; Shen, K.; Ding, D.; Chen, J.; Fan, T.; Wu, R.; Li, Y. Solvent-Driven Selectivity Control to either Anilines or Dicyclohexylamines in Hydrogenation of Nitroarenes over a Bifunctional Pd/MIL-101 Catalyst. *ACS Catal.* **2018**, *8*, 10641−10648.
(56) Xu, C.; Fang, R.; Luque, R.; Chen, L.; Li, Y. Functional metal−organic frameworks for catalytic applications. *Coord. Chem. Rev.* **2019**, *388*, 268−292.
(57) Leandro, S. R.; Mourato, A. C.; Łapińska, U.; Monteiro, O. C.; Fernandes, C. I.; Vaz, P. D.; Nunes, C. D. Exploring bulk and colloidal Mg/Al hydrotalcite−Au nanoparticles hybrid materials in aerobic olefin epoxidation. *J. Catal.* **2018**, *358*, 187−198.
(58) Gao, W.-Y.; Wojtas, L.; Ma, S. A porous metal−metalloporphyrin framework featuring high-density active sites for chemical fixation of CO_2 under ambient conditions. *Chem. Commun.* **2014**, *50*, 5316−5318.
(59) He, H.; Sun, Q.; Gao, W.; Perman, J. A.; Sun, F.; Zhu, G.; Aguila, B.; Forrest, K.; Space, B.; Ma, S. A stable metal−organic framework featuring a local buffer environment for carbon dioxide fixation. *Angew. Chem., Int. Ed.* **2018**, *57*, 4657−4662.

https://dx.doi.org/10.1021/acs.inorgchem.9b02952
Inorg. Chem. XXXX, XXX, XXX−XXX